

Pressure-induced high-temperature superconductivity retained at ambient

Liangzi Deng^{1,*}, Trevor Bontke¹, Rabin Dahal¹, Yu Xie², Bin Gao³, Xue Li², Ketao Yin⁴,
Melissa Gooch¹, Donald Rolston¹, Tong Chen³, Zheng Wu¹, Yanming Ma², Pengcheng Dai³, and
Ching-Wu Chu^{1,5,*}

¹Department of Physics and Texas Center for Superconductivity, University of Houston,
Houston, TX

²International Center for Computational Method and Software and State Key Laboratory of
Superhard Materials, College of Physics, Jilin University, Changchun, China

³Department of Physics and Astronomy, Rice University, Houston, TX

⁴School of Physics and Electronic Engineering, Linyi University, Linyi, Shandong, China

⁵Lawrence Berkeley National Laboratory, Berkeley, CA

*Corresponding authors: ldeng2@central.uh.edu and cwchu@uh.edu

To raise the superconducting-transition temperature (T_c) has been the driving force for the long, sustained effort in superconductivity research. Recent progress in hydrides¹⁻³ with T_c s up to 287 K under 267 GPa has heralded a new era of room-temperature superconductivity (RTS) with immense technological promise. Indeed, RTS has lifted the temperature barrier for the ubiquitous application of superconductivity. Unfortunately, formidable pressure is required to attain such high T_c s. The most effective relief to this impasse is to remove the pressure needed while retaining the pressure-induced T_c without pressure. Here we show such a possibility in the pure and doped high-temperature superconductor (HTS) FeSe by retaining, at ambient via pressure-

quenching (PQ), its T_c up to 37 K (quadrupling that of a pristine FeSe⁴) and other pressure-induced phases⁵. We have also observed that some phases remain stable without pressure at up to 300 K and for at least 7 days. The observations are in qualitative agreement with our *ab initio* simulations using the solid-state nudged elastic band (SSNEB) method⁶. We strongly believe that the PQ technique developed here can be adapted to the RTS hydrides and other materials⁷⁻¹¹ of value with minimal effort.

The vast impact of RTS on humanity is limited only by the imagination. Recent reports show that RTS is indeed within reach, although only under high pressure (HP). For instance, T_c s above 200 K have been reported in unstable molecular solids (hydrides), i.e., up to 203 K in H₃S under 155 GPa¹, up to 260 K in LaH₁₀ under 190 GPa², and up to 287 K in C-H-S under 267 GPa³; earlier, T_c up to 164 K was reported in the stable cuprate HTS HgBa₂Ca₂Cu₃O_{8+ δ} under 31 GPa^{7,8}. The challenge now shifts from raising the T_c to lowering, and better yet removing, the applied pressure (P_A) required. Retaining the pressure-induced high- T_c superconducting (SC) phase without pressure will effectively meet this challenge.

It has been shown that most of the alloys used in industrial applications are actually metastable at room temperature and atmospheric pressure¹². These metastable phases, such as diamond and black phosphorus, possess desired and/or enhanced properties that their stable counterparts lack. They are metastable because they are kinetically stable but thermodynamically not, protected only by an energy barrier (Extended Data Fig. 1). By taking advantage of such energy barriers, lattice and/or electronic, one may therefore be able to stabilize the metastable phase or the “supercool” state at atmospheric pressure via rapid pressure- and/or temperature-quenching. The

energy barrier may be fortified by chemical doping; a proper thermodynamic path; and introduction of strains, defects, or pressure inhomogeneity¹³. The pressure-enhanced or -induced SC phase with a high T_c may be considered metastable or supercool and may be stabilized. Last year we retained two SC phases with $T_{cs} \sim 3.4$ K and 4.0 K from 9 and 30 GPa, respectively, in non-SC elemental Sb¹⁴. Here we report the first successful retention of pressure-enhanced and -induced SC phases at ambient in the Fe-based HTSs via PQ at a chosen quench-pressure (P_Q) and quench-temperature (T_Q), i.e., a pressure-enhanced SC phase with a T_c up to 37 K at $P_Q = 4.15$ GPa and $T_Q = 4.2$ K in the SC FeSe and a pressure-induced SC phase with a T_c up to 26.5 K at $P_Q = 6.32$ GPa and $T_Q = 4.2$ K in the non-SC Cu-doped FeSe. We have also successfully retained the insulating phase induced by pressure above ~ 9 GPa in both samples via PQ. The pressure-quenched (PQed) high- T_c phases have also been found to be stable up to ~ 200 K and for at least 7 days. Our observations have thus demonstrated that the pressure-enhanced or -induced high- T_c phases in HTSs can be retained at ambient via PQ at a chosen P_Q and T_Q , suggesting a possible realistic path to the ubiquitous applications of the recently reported RTS.

In the present study, we have chosen single crystals of the SC FeSe⁴ and the non-SC Cu-doped FeSe¹⁵ as model HTSs due to their simple structure and chemistry, as well as their large T_c variation under pressure^{5,16} and their important role in unraveling HTS¹⁷⁻¹⁹. Their normalized resistance at 300 K as a function of pressure [$R(P_A)/R(0)$] during pressure-increasing and -decreasing is displayed in Extended Data Fig. 2, which shows a clear hysteresis, suggesting that PQ may be possible. Preliminary boundaries of the orthorhombic (O) – tetragonal (T) – hexagonal (H) phase transitions of FeSe previously reported^{16,20} are also shown for later discussion. The T-O transition is suppressed from ~ 90 K at ambient to below 4.2 K at ~ 2 GPa,

as indicated by the dashed line at left in the same figure. At ambient, $R(T)$ of FeSe shows a sharp SC transition at 9 K (Extended Data Fig. 3a). The transition broadens under pressure, so the $T_c(P)$ cited hereafter refers to the onset temperature as defined. Figure 1 (blue squares) displays the T_c -variation of FeSe with P_A : it increases slowly from ~ 9 K at 0 GPa to ~ 15 K below 1.9 GPa; suddenly jumps to ~ 32 K at 1.9 GPa, coinciding with the O-T transition; continues to rise with a broad peak at ~ 40 K around ~ 4 GPa; but finally becomes insulating above ~ 8 GPa as the H phase sets in.

To retain at ambient the above pressure-enhanced T_c of FeSe, we have developed a technique to PQ the sample at different P_{QS} and T_{QS} by rapidly removing the P_A , under which a desired T_c has been first attained, from the sample in the diamond anvil cell (DAC), as shown in Figs. 2a-f. The temperature-dependent resistance of FeSe at different P_{AS} normalized to those at 70 K, $R(T, P_A)/R(70 \text{ K}, P_A)$, near the superconducting transitions are exemplified in Figs. 2a-b for $P_{AS} = 4.15$ GPa (*close to maximum $T_c \sim 40$ K in the tetragonal phase*), and 11.27 GPa (*non-SC in the hexagonal phase*), respectively. By following different thermal and pressure protocols as specified in the captions, they demonstrate the generation or destruction of the HP SC phase at P_A (blue), the retention at ambient of the PQed (at 4.2 K) HP SC phase (red), and the thermal annealing effect up to 300 K on the PQed (at 4.2 K) HP phase to ascertain its retention (orange), all carried out sequentially.

As is evident from Fig. 2a, the T_c of the FeSe sample has been enhanced from 9 K at ambient to ~ 39 K under ~ 4.15 GPa (blue). After PQ at 4.15 GPa and 4.2 K, a SC transition with a $T_c \sim 37$ K is detected at ambient (red). To show that the 37 K- T_c is indeed attained by PQ, we heated the

sample up to 300 K before cooling it back down to 4.2 K and found that the PQed SC transition at 37 K is annealed away and replaced by its pre-PQed one, although at a higher $T_c \sim 20$ K (orange) rather than 9 K, presumably because of an unknown irreversible residual strain effect in the sample²¹. Figure 2b shows that FeSe at 11.27 GPa displays a non-SC transition as expected (blue), as does the PQed sample (red). However, the sample regains its SC transition with a $T_c \sim 20$ K after the PQed phase is annealed off after being heating up to 300 K (orange). To demonstrate the metastability of the PQed SC phases, the SC transition PQed at $P_Q = 4.13$ GPa and $T_Q = 4.2$ K upon sequential thermal cycling to higher temperatures is shown in Fig. 2c. The transition is smoothly shifted downward and becomes sharper (due to the reduced fluctuations at lower temperature). The sudden downward shift in the overall SC transition by ~ 10 K after heating up to ~ 200 K implies that the PQed phase transforms to the pre-PQed FeSe phase (with strain) and is stable up to 200 K. All T_c s of the PQed phases examined at different P_Q s and $T_Q = 4.2$ K are summarized in Fig. 1 (red circles).

As mentioned earlier, the PQed phase is metastable, and thus should depend on P_Q and T_Q and detailed electronic and phonon energy spectra of the materials examined. We have therefore repeated the PQ experiments on FeSe by raising only the T_Q to 77 K (Fig. 2d-f). Figure 2d shows that the T_c of FeSe before PQ has been enhanced to ~ 37 K at 5.22 GPa (blue); upon PQ, a $T_c \sim 24$ K is retained at ambient (green) in contrast to the 37 K when $T_Q = 4.2$ K, as shown in Fig. 2a; and the transition returns to ~ 14 K on cooling after warming to 300 K, showing that the 24 K transition is associated with the PQed phase. Figure 2e shows that FeSe becomes insulating at 11.12 GPa (blue); the phase is retained at ambient by PQ (green); and the PQed phase remains after heating to 300 K, suggesting that this PQed non-SC phase is stable up to 300 K. The effect

of systematic thermal cycling with increasing temperatures on the PQed phase at $P_Q = 11.12$ GPa and $T_Q = 77$ K is shown in Fig. 2f. All T_{cs} of the PQ phases examined at different P_Q s and $T_Q = 77$ K are also summarized in Fig. 1 (green diamonds). They are all lower than those quenched at $T_Q = 4.2$ K in general agreement with the competition between the instability of the SC state and thermal excitation.

To avoid possible confusion of the SC state of the pristine FeSe with that of the SC PQed FeSe, we have investigated the Cu-doped FeSe [(Fe_{0.98}Cu_{0.03})Se], which is not SC above 1.2 K in its uncompressed state^{5,15}, as shown in Extended Data Fig. 3b. Under pressure [Fig. 3 (blue squares)], it abruptly becomes SC with a $T_c \sim 20$ K at 3.11 GPa (inset, Extended Data Fig. 3b); T_c continues to increase with increasing P_A and peaks at ~ 27 K under 6.23 GPa; and at 9.65 GPa, only trace superconductivity was detected down to 1.2 K. Following the same protocols as those for the pure FeSe, we performed PQ on Cu-doped FeSe at different P_Q s and T_Q s, as shown in Figs. 4a-f. Two examples of $R(T, P_A)_s / R(50 \text{ K}, P_A)$ for Cu-doped FeSe are given in Fig. 4a for $P_{As} = 6.32$ GPa and 6.16 GPa (*close to maximum $T_c \sim 27$ K*) PQed at $T_Q = 4.2$ K and 77 K, respectively; and in Fig. 4b for 9.65 GPa (*non-SC*) PQed at $T_Q = 77$ K. As is evident from the $R(T, P_A)_s / R(50 \text{ K}, P_A)$ in Fig. 4a, $P_A \sim 6$ GPa has induced a SC state in the non-SC Cu-doped FeSe with a $T_c \sim 26$ K (navy and blue); this SC state has been PQed at $P_Q = 6.16$ GPa and $T_Q = 4.2$ K (red) and at $P_Q = 6.32$ GPa and $T_Q = 77$ K (green), respectively. Disappearance of the SC phase after thermal cycling up to 300 K (Fig. 4a, orange and brown) demonstrates that the SC states induced by $P_A \sim 6$ GPa have been retained at ambient with $T_c \sim 26$ K via PQ at 4.2 K and 77 K, respectively. As shown in Fig. 4b, $P_A = 9.65$ GPa turns the sample to an insulating state (blue); upon PQ at $T_Q = 77$ K it becomes insulating (green); and the sample remains in the non-

SC state after thermal cycling to 300 K (orange), suggesting that the insulating state PQed at 9.65 GPa and 77 K is stable up to 300 K. The thermal stability ranges of the PQed SC states at $P_Q = 6.08$ GPa and $T_Q = 4.2$ K and at $P_Q = 5.95$ GPa and $T_Q = 77$ K are shown in Figs. 4c and 4d, respectively. They show that the state PQed at a lower T_Q possesses a wider thermal stability range. The anomalies observed in $R(T)$ upon warming right after PQ (Fig. 4e) correlate qualitatively with the thermal stability of the PQed phases (Figs. 4c-d). Figure 4f demonstrates that the PQed SC phase at $P_Q = 6.67$ GPa and $T_Q = 77$ K remains unchanged for at least 7 days after thermal cycling between 50 K and 4.2 K. All PQed T_c s of Cu-doped FeSe are summarized in Fig. 3. Unlike in their pristine unpressured state, the two different Cu-doped FeSe samples both behave similarly to FeSe under pressures, but with their phase boundaries shifted to higher values, as displayed in Figs. 1 and 3 and Extended Data Fig. 4, due to the Cu-doping effect. While PQ works for both pure and Cu-doped FeSe in retaining at ambient the pressure-enhanced or -induced SC states, the effect of T_Q on the T_c of the PQed SC phase for Cu-doped FeSe is smaller than that for FeSe, due to the possible change in the electronic structure resulting from doping. This suggests that doping can help adjust the quenching parameters.

To gain a better understanding of the PQ effects on FeSe, we performed *ab initio* simulations to evaluate the phase transition energy barriers between different phases via SSNEB⁶. As shown in Extended Data Fig. 5a-b, the phase transition energy barrier between the orthorhombic²² and tetragonal²³ phases is small. For instance, the energy barrier is 3 meV/atom at 6 GPa, which is lower than the energy barrier of 6 meV/atom at 0 GPa, suggesting that the transition temperature between these two phases at HP should be lower than that at ambient, in agreement with the experimental observations. Nevertheless, the small energy barrier between those two structures

ensures that FeSe could preserve the structure phase from one transfer to the other when PQed from above 2 GPa to ambient at low temperatures, as well as the superconductivity. On the other hand, the phase transition energy barrier from the hexagonal²⁴ to the tetragonal phase is significantly larger, about 0.189 and 0.193 eV/atom at 8 and 11 GPa, respectively (Extended Data Fig. 5c-d). We also noticed that the tetragonal phase is energetically more favorable than the hexagonal phase at simulated pressures. The phase transition between the tetragonal and hexagonal phases will occur at 15 GPa based on our simulation, in agreement with previous calculations²⁵. The estimated energy barriers are comparable to that between graphite and cubic diamond, around 0.21 eV/atom at 10 GPa²⁶, suggesting that the hexagonal phase could be preserved during the quenching process once it is formed, as we observed in our experiments. The energy barrier is high enough to prevent FeSe returning to the orthorhombic phase from the hexagonal phase at ambient pressure and 300 K, which is consistent with our experiments at $P_Q = 11.12$ GPa and $T_Q = 77$ K shown in Fig. 2e.

In conclusion, we have demonstrated that the pressure-induced/enhanced superconducting phases with high T_c and the pressure-induced semiconducting phases in FeSe and Cu-doped FeSe can be stabilized at ambient without pressure by pressure-quenching at chosen pressures and temperatures. These pressure-quenched phases have been shown to be stable at up to 300 K and for up to at least 7 days. The observations suggest that the recently reported room-temperature superconductivity in hydrides close to 300 GPa may be retained without pressure, making possible the ubiquitous applications of superconductivity envisioned.

References

1. Drozdov, A. P., Eremets, M. I., Troyan, I. A., Ksenofontov, V. & Shylin, S. I. Conventional superconductivity at 203 kelvin at high pressures in the sulfur hydride system. *Nature* **525**, 73 (2015).
2. Somayazulu, M. et al. Evidence for Superconductivity above 260 K in Lanthanum Superhydride at Megabar Pressures. *Phys. Rev. Lett.* **122**, 027001 (2019).
3. Snider, E. et al. Room-temperature superconductivity in a carbonaceous sulfur hydride. *Nature* **586**, 373 (2020).
4. Wu, M. K. et al. Superconductivity in the PbO-type structure α -FeSe. *Proc. Natl. Acad. Sci. U.S.A.* **105**, 14262 (2008).
5. Schoop, L. M. et al. Pressure-restored superconductivity in Cu-substituted FeSe. *Phys. Rev. B* **84**, 174505 (2011).
6. Sheppard, D., Xiao, P. H., Chemelewski, W., Johnson, D. D. & Henkelman, G. A generalized solid-state nudged elastic band method. *J. Chem. Phys.* **136**, 074103 (2012).
7. Chu, C.W. et al. Superconductivity above 150 K in $\text{HgBa}_2\text{Ca}_2\text{Cu}_3\text{O}_{8+\delta}$ at high pressures. *Nature* **365**, 323 (1993).
8. Gao, L. et al. Superconductivity up to 164 K in $\text{HgBa}_2\text{Ca}_{m-1}\text{Cu}_m\text{O}_{2m+2+\delta}$ ($m = 1, 2, \text{ and } 3$) under quasihydrostatic pressures. *Phys. Rev. B* **50**, 4260 (R) (1994).
9. Chen, X. J. et al. Enhancement of superconductivity by pressure-driven competition in electronic order. *Nature* **466**, 950 (2010).
10. Sun, L. L. et al. Re-emerging superconductivity at 48 Kelvin in iron chalcogenides. *Nature* **483**, 67 (2012).
11. Deng, L. Z. et al. Higher superconducting transition temperature by breaking the universal pressure relation. *Proc. Natl. Acad. Sci. USA* **116**, 2004 (2019).

12. Duwez, P. Metastable phases obtained by rapid quenching from the liquid state. *Prog. Solid. State Ch.* **3**, 377 (1967).
13. Zhang, F. X. & Wang, W. K. Crystal structure of germanium quenched from the melt under high pressure. *Phys. Rev. B* **52**, 3113 (1995).
14. Wu, Z., Deng, L. Z., Gooch, M., Huyan, S. & Chu, C. W. The retention at ambient of the high-pressure-induced metastable superconducting phases in antimony single crystals. *Mater. Today Phys.* **15**, 100291 (2020).
15. Williams, A. J., McQueen, T. M., Ksenofontov, V., Felser, C. & Cava, R. J. The metal-insulator transition in $\text{Fe}_{1.01-x}\text{Cu}_x\text{Se}$. *J. Phys.: Condens. Matter* **21**, 205701 (2009).
16. Medvedev, S. *et al.* Electronic and magnetic phase diagram of $\beta\text{-Fe}_{1.01}\text{Se}$ with superconductivity at 36.7 K under pressure. *Nat. Mater.* **8**, 630 (2009).
17. Wang, Q. Y. *et al.* Interface-Induced High-Temperature Superconductivity in Single Unit-Cell FeSe Films on SrTiO_3 . *Chin. Phys. Lett.* **29**, 037402 (2012).
18. He, S. L. *et al.* Phase diagram and electronic indication of high-temperature superconductivity at 65 K in single-layer FeSe films. *Nat. Mater.* **12**, 605 (2013).
19. Deng, L. Z. *et al.* Meissner and mesoscopic superconducting states in 1 - 4 unit-cell FeSe films. *Phys. Rev. B* **90**, 214513 (2014).
20. Miyoshi, K. *et al.* Enhanced Superconductivity on the Tetragonal Lattice in FeSe under Hydrostatic Pressure. *J. Phys. Soc. Jpn.* **83**, 013702 (2014).
21. Locquet, J. P. *et al.* Doubling the critical temperature of $\text{La}_{1.9}\text{Sr}_{0.1}\text{CuO}_4$ using epitaxial strain. *Nature* **394**, 453 (1998).
22. Horigane, K., Hiraka, H. & Ohoyama, K. Relationship between Structure and Superconductivity in $\text{FeSe}_{1-x}\text{Te}_x$. *J. Phys. Soc. Jpn.* **78**, 074718 (2009).

23. Haegg, G. & Kindstroem, A. L. Roentgenuntersuchungen am system Eisen-Selen. *Z. Phys. Chem. B.* **22**, 453 (1933).
24. Kamimura, T. *et al.* Pressure-induced phase transition in Fe-Se and Fe-S systems with a NiAs-type structure. *J. Magn. Magn. Mater.* **104**, 255 (1992).
25. Lu, C. *et al.* Theoretical investigation on the structural and thermodynamic properties of FeSe at high pressure and high temperature. *Dalton Trans.* **41**, 9781 (2012).
26. Dong, X. *et al.* An ab initio study on the transition paths from graphite to diamond under pressure. *J. Phys.: Condens. Matter* **25**, 145402 (2013).

Figures and legends

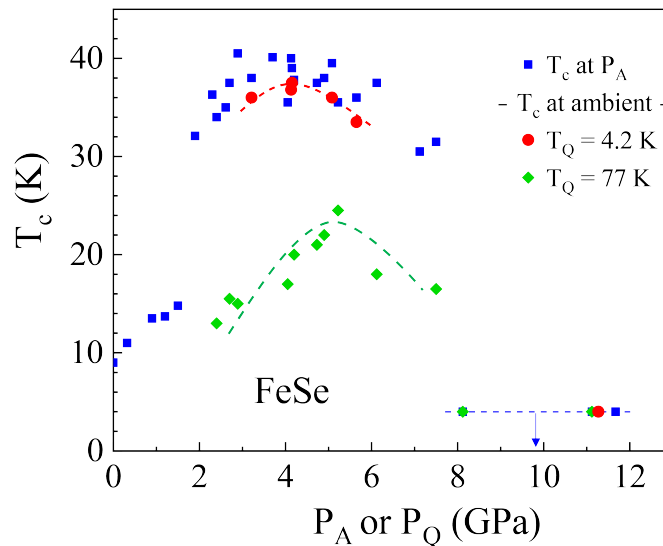


Fig. 1 | T_c as a function of P_A or P_Q for single-crystalline FeSe. High-pressure T_c (P_A) at P_A (blue squares), and T_c (P_Q) at ambient for FeSe PQed at P_Q and $T_Q = 4.2$ K (red circles) and $T_Q = 77$ K (green diamonds), respectively.

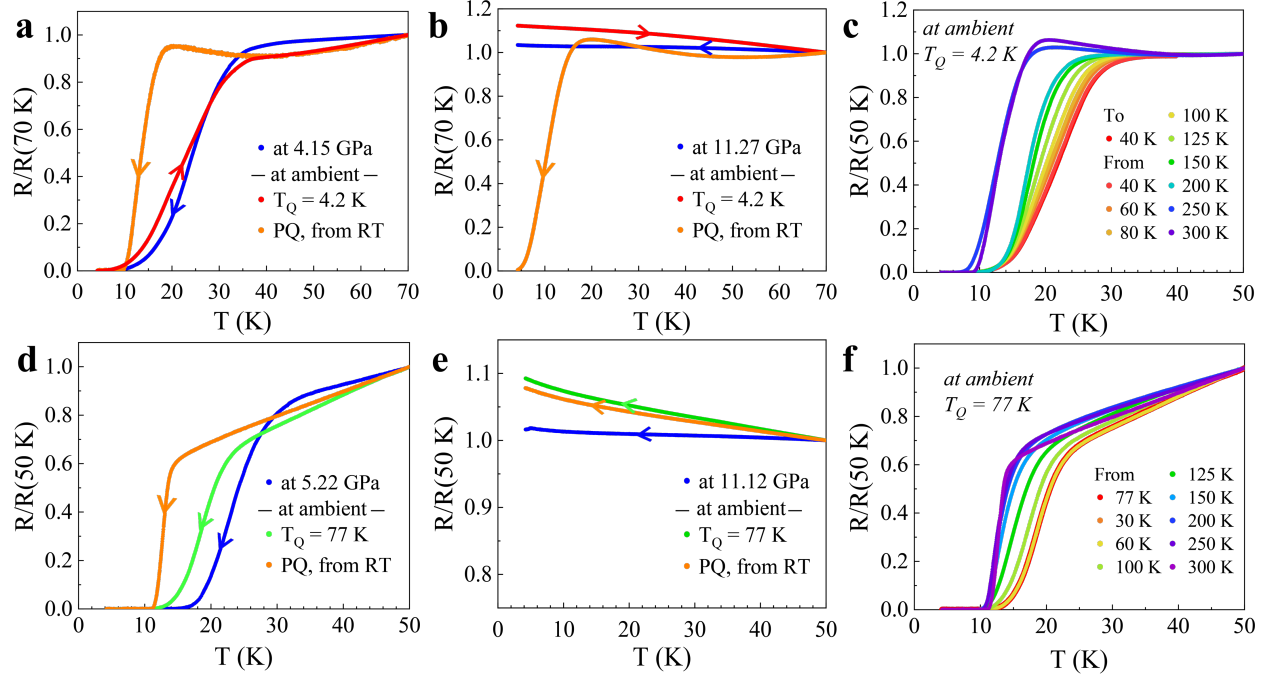


Fig. 2 | Pressure-quenching the single-crystalline FeSe. $R(T)/R(70\text{ K})$ or $R(T)/R(50\text{ K})$ under P_A and at ambient after PQ: **a.** at $P_A = 4.15\text{ GPa}$ (blue), and at ambient after PQ at 4.15 GPa and 4.2 K on warming (red) and on cooling after warming to 300 K (orange); **b.** at $P_A = 11.27\text{ GPa}$ (blue), and at ambient after PQ at 11.27 GPa and 4.2 K on warming (red) and on cooling after warming to 300 K (orange); **c.** after PQ at 4.13 GPa and 4.2 K, sequential thermal cycling up to 300 K; **d.** at $P_A = 5.22\text{ GPa}$ (blue), and at ambient after PQ at 5.22 GPa and 77 K on cooling (green) and on cooling after warming to 300 K (orange); **e.** at $P_A = 11.12\text{ GPa}$ (blue), and at ambient after PQ at 11.12 GPa and 77 K on cooling (green) and on cooling after warming to 300 K (orange); and **f.** after PQ at 5.22 GPa and 77 K, sequential thermal cycling up to 300 K.

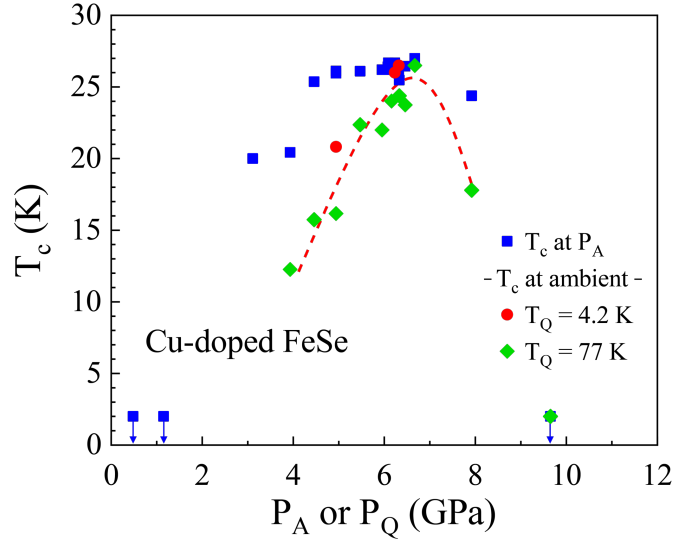


Fig. 3 | T_c as a function of P_A or P_Q for single-crystalline Cu-doped FeSe. $T_c(P_A)$ at P_A (blue squares); and at $T_c(P_Q)$ at ambient for the samples PQed at P_Q and $T_Q = 4.2$ K (red circles) and at $T_Q = 77$ K (green diamonds), respectively.

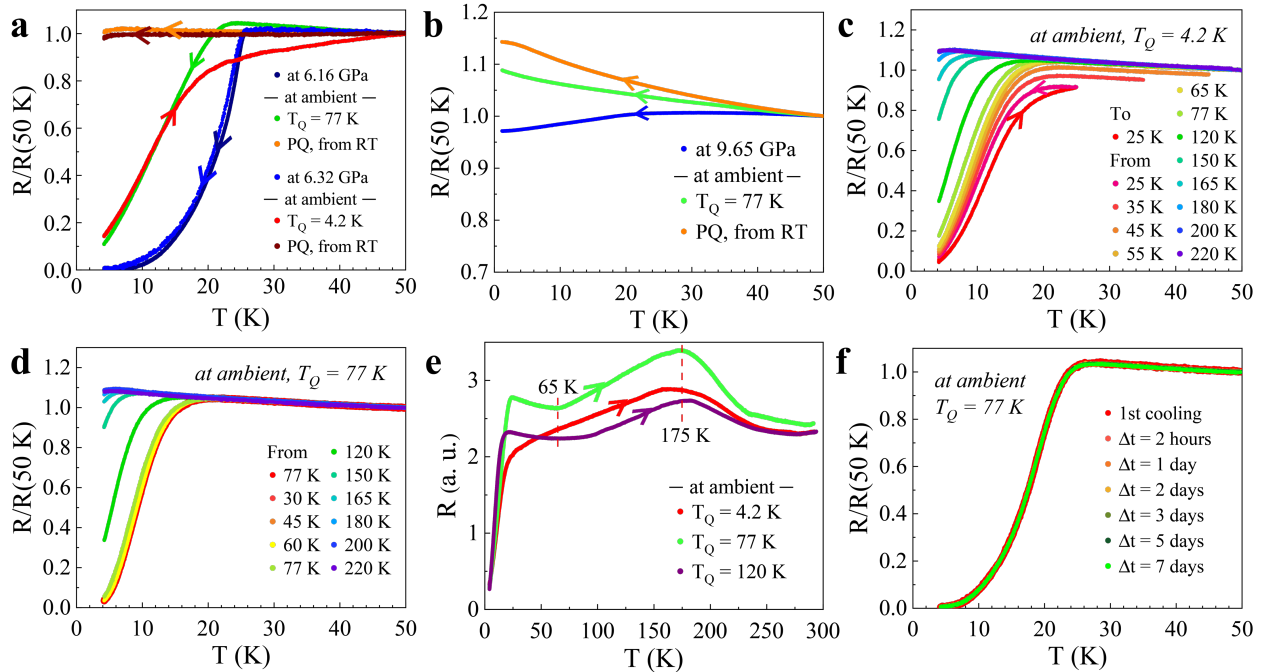


Fig. 4 | Pressure-quenching the single-crystalline Cu-doped FeSe. $R(T)/R(50\text{ K})$ under P_A and at ambient after PQ, and testing the stability of the PQed phases: **a.** at $P_A = 6.16$ GPa (navy) and

6.32 GPa (blue), and at ambient after PQ at 6.16 GPa and 77 K (green), and at 6.32 GPa and 4.2 K (red), and on cooling after warming to 300 K (orange and brown); **b.** at $P_A = 9.65$ GPa (blue), at ambient after PQ at 9.65 GPa and 77 K (green), and on cooling after warming to 300 K (orange); **c.** at ambient after PQ at 6.08 GPa and 4.2 K, sequential thermal cycling up to 220 K; **d.** at ambient after PQ at 5.95 GPa and 77 K, sequential thermal cycling up to 220 K; **e.** $R(T)$ at ambient for the same sample subjected to different PQ conditions: $P_Q = 6.31$ GPa and $T_Q = 4.2$ K (red), $P_Q = 6.16$ GPa and $T_Q = 77$ K (green), and $P_Q = 6.51$ GPa and $T_Q = 120$ K (purple); and **f.** repeated thermal cycling at ambient from 50 K for the sample PQed at 6.67 GPa and 77 K.

Methods

Single crystals of $\text{Fe}_{1.01-x}\text{Cu}_x\text{Se}$ ($x = 0, 0.03, \text{ and } 0.035$) were grown using the chemical vapor transport (CVT) method²⁷. Stoichiometric high-purity Fe, Cu, and Se powders were thoroughly mixed and loaded into a quartz tube. AlCl_3 and KCl powders were added as the transport agents. After the evacuated quartz tube was sealed, it was placed into a two-zone tube furnace, in which the temperatures of the hot and cold positions were maintained at 420 °C and 330 °C, respectively. After 20 days, single crystals with an average size of $3 \times 3 \times 0.1$ mm³ were grown around the region of the quartz tube's cold zone. Chemical composition was determined by energy-dispersive spectroscopy (EDS) using a Tescan Lyra scanning electron microscope (SEM) equipped with an EDS detector (Oxford Instruments).

For resistivity measurements conducted in this investigation, pressure was applied to the samples using a symmetric-type diamond anvil cell with a culet size of 500 μm . The stainless-steel gasket was insulated with Stycast 2850. The sample's chamber diameter is 250 μm , where either

sodium chloride or cubic boron nitride is used as the pressure medium. Samples were cut into thin squares with a diagonal of $\sim 180 \mu\text{m}$ and thickness of $\sim 10 \mu\text{m}$. The pressure was determined using the ruby fluorescence scale or the diamond Raman scale at room temperature. The samples' contacts were arranged in a Van der Pauw configuration and data were collected using a Keithley 2182A/6221 low-resistance measurement setup. Measurements were conducted in a homemade cooling system that can be cooled to 1.2 K by pumping on the liquid-helium space. Pressure-quenching was performed by releasing the screws at target temperatures with a small residual pressure $P_R < 0.2 \text{ GPa}$ to maintain the electrical connectivity for resistivity measurements, and the P_R was measured at room temperature.

Our calculations were performed within the framework of density functional theory via the generalized gradient approximation GGA + U method implemented in the Vienna ab initio simulation package (VASP)²⁸. The electron-ion interactions were represented by means of the all-electron projector augmented wave (PAW) method²⁹, where $3d^64s^2$ and $4s^24p^4$ are treated as the valence electrons for Fe and Se, respectively. We used the Dudarev implementation³⁰ with on-site coulomb interaction $U = 5.0 \text{ eV}$ and on-site exchange interaction $J = 0.8 \text{ eV}$ ³¹ to treat the localized 3d electron states. The Perdew-Burke-Ernzerhof (PBE) functional in the generalized gradient approximation (GGA) was used to describe the exchange-correlation potential^{32,33}. The plane-wave energy cutoff of 400 eV and a dense k-point grid of spacing $2\pi \times 0.03 \text{ \AA}^{-1}$ in the Monkhorst-Pack scheme were used to sample the Brillouin zone. Structural relaxations were performed with forces converged to less than 0.05 eV \AA^{-1} . To determine the energy barriers, we used the solid-state nudged elastic band method (SSNEB)⁶ implemented in VASP. The NEB path was first constructed by linear interpolation of the atomic coordinates and then relaxed until

the forces on all atoms were < 0.05 eV/Å. Seven images were simulated between the initial and final states.

Methods References

27. Chareev, D. *et al.* Single crystal growth and characterization of tetragonal FeSe_{1-x} superconductors. *Cryst. Eng. Commun.* **15**, 1089 (2013).
28. Kresse, G. & Furthmüller, J. Efficient iterative schemes for ab initio total-energy calculations using a plane-wave basis set. *Phys. Rev. B* **54**, 11169 (1996).
29. Blöchl, P. E. Projector augmented-wave method. *Phys. Rev. B* **50**, 17953 (1994).
30. Dudarev, S. L., Botton, G. A., Savrasov, S. Y., Humphreys, C. J. & Sutton, A. P. Electron-energy-loss spectra and the structural stability of nickel oxide: An LSDA+U study. *Phys. Rev. B* **57**, 1505 (1998).
31. Zhang, J. *et al.* Rare Helium-Bearing Compound FeO₂He Stabilized at Deep-Earth Conditions. *Phys. Rev. Lett.* **121**, 255703 (2018).
32. Perdew, J. P. & Wang, Y. Accurate and simple analytic representation of the electron-gas correlation energy. *Phys. Rev. B* **45**, 13244 (1992).
33. Perdew, J. P., Burke, K. & Ernzerhof, M. Generalized Gradient Approximation Made Simple. *Phys. Rev. Lett.* **77**, 3865 (1996).

Author contributions

C.-W.C., L. D., and Z.W. conceived, developed, and executed the original idea of pressure-quenching. L.D., T.B., R.D., M.G., and D.R. acquired data. L.D., T.B., and C.-W.C. analyzed the

data. B.G., T.C., and P.D. grew the samples. Y.X., X.L., K.Y., Z.W., and Y.M. provided theoretical interpretation. C.-W.C., L.D., and Z.W. provided overall supervision.

Acknowledgments

We thank Prof. L. L. Sun, C. Huang, and J. Guo at IoP, CAS, for efforts on the synchrotron X-ray experiments under high pressure at beamline 4W2 of the Beijing Synchrotron Radiation Facilities. The work performed at the Texas Center of Superconductivity at the University of Houston is supported by US Air Force Office of Scientific Research Grant FA9550-15-1-0236 and FA9550-20-1-0068, the T. L. L. Temple Foundation, the John J. and Rebecca Moores Endowment, and the State of Texas through the Texas Center for Superconductivity at the University of Houston. The FeSe and Cu-doped FeSe single crystal growth work at Rice University is supported by the US Department of Energy, Basic Energy Sciences, under Contract No. DE-SC0012311 (P.D.).

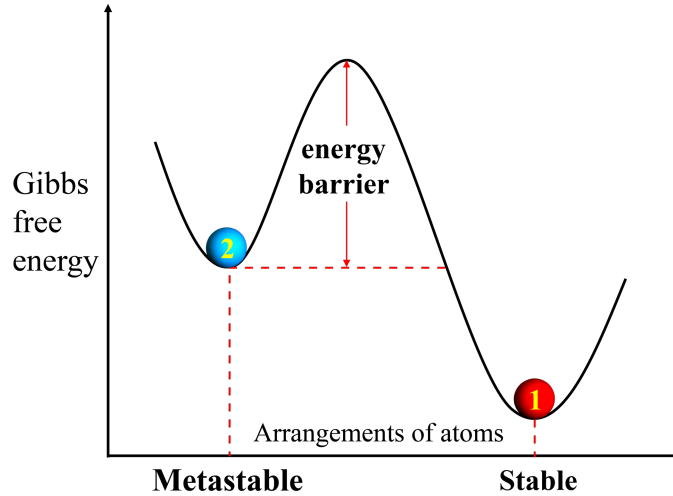
Competing interest declaration

The authors declare no competing interests.

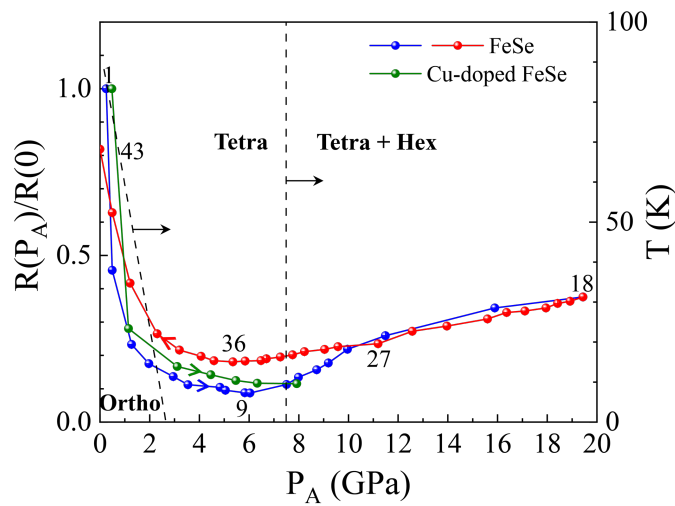
Data availability

All data that support the findings of this study are available from the corresponding authors on request.

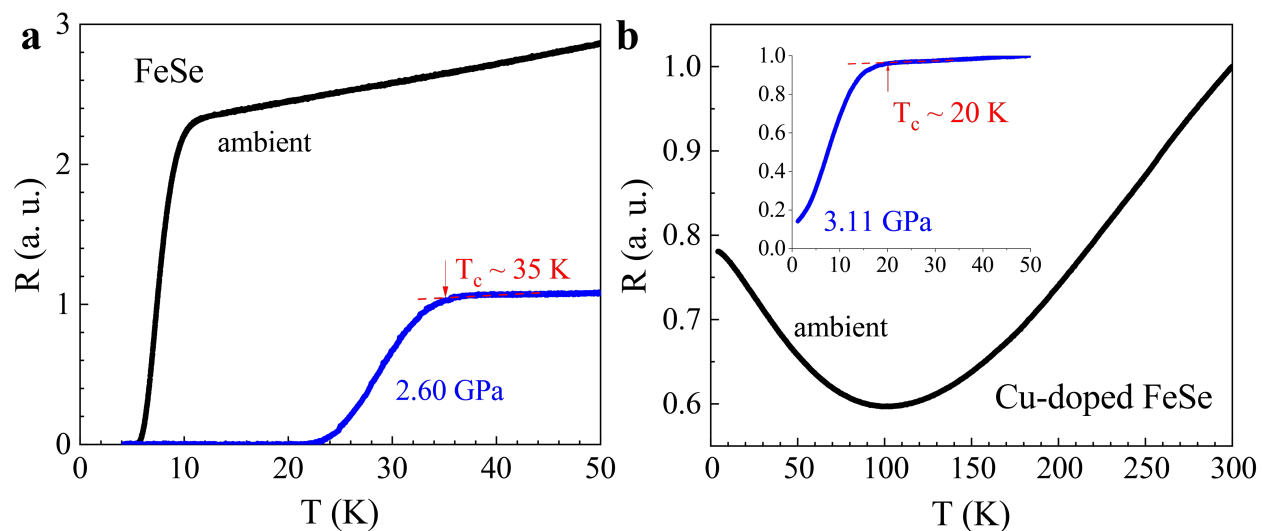
Extended Data



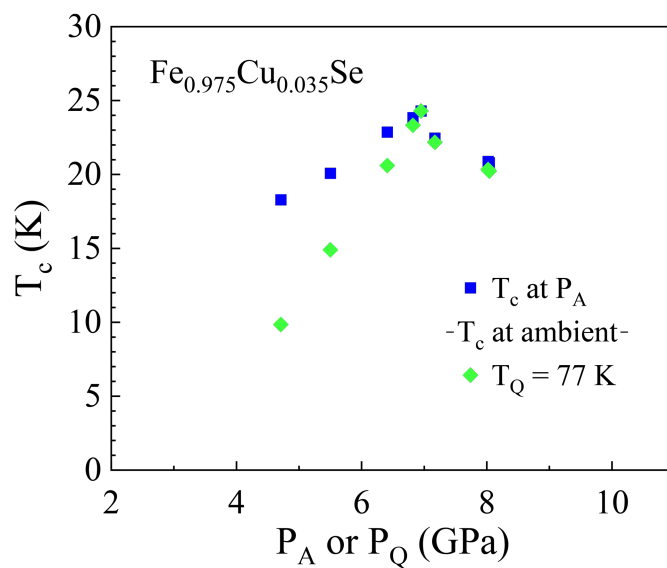
Extended Data Fig. 1 | Schematic diagram of Gibbs free energy and the energy barrier between the metastable and stable states.



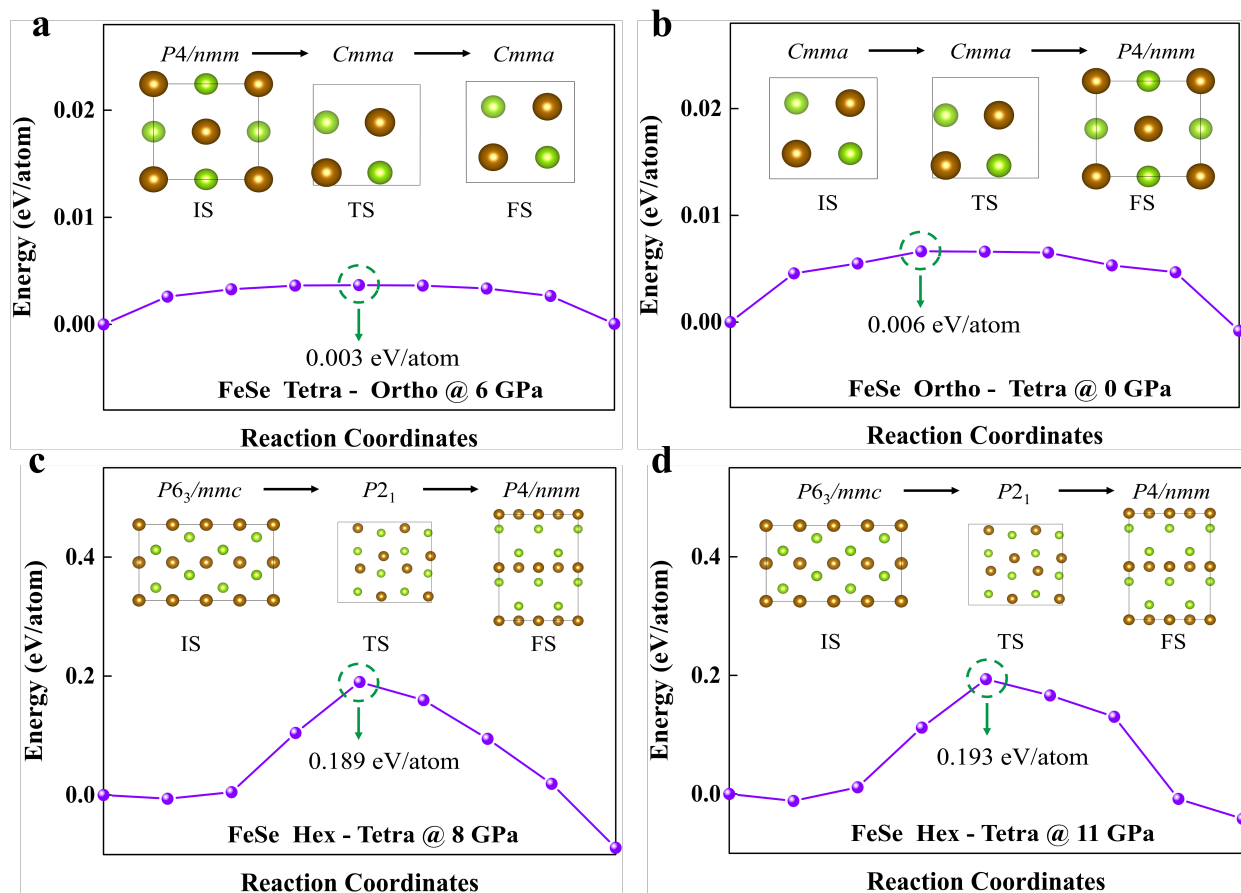
Extended Data Fig. 2 | $R(P_A)/R(0)$ of FeSe and Cu-doped FeSe single crystals at 300 K during pressure cycling. Dashed lines represent phase boundaries for FeSe^{16,20}. Numbers denote the sequential order of the experimental runs.



Extended Data Fig. 3 | Resistance as a function of temperature for FeSe and Cu-doped FeSe single crystals. a, FeSe at ambient (black) and at 2.60 GPa (blue). **b,** Cu-doped FeSe at ambient and (inset) at 3.11 GPa. Red dashed lines and arrows define the T_c .



Extended Data Fig. 4 | T_c as a function of P_A or P_Q for single-crystalline Cu-doped FeSe. High-pressure T_c (P_A) at P_A (blue squares); and T_c (P_Q) at ambient for Cu-doped FeSe sample PQed at P_Q and $T_Q = 77$ K (green diamonds).



Extended Data Fig. 5 | Energy barrier between different phases of FeSe. Calculated energy barrier from **a**, the tetragonal phase to the orthorhombic phase at 6 GPa and **b**, the orthorhombic phase to the tetragonal phase at 0 GPa. Calculated energy barrier from the hexagonal phase to the tetragonal phase at **c**, 8 GPa and **d**, 11 GPa. Insets show the side views of corresponding structures including the initial state (IS), the transition state (TS), and the final state (FS) along the *c* axis. The energy barrier was calculated through the solid-state nudged elastic band method in which seven images were used. The arrows show the transition state that is the image with the highest energy and the estimated energy barrier. The green and brown spheres represent elemental Se and Fe, respectively.